# Transformation process dependent magnetocaloric properties of annealed Ni$_{50}$Mn$_{18}$Cu$_7$Ga$_{25}$ ribbons

Naifu Zou[1, 2], Zongbin Li[1], Yudong Zhang[2, 3], C.F. Sánchez-Valdés[4], J.L. Sánchez Llamazares[5, *], Claude Esling[2, 3], Bo Yang[1], Xiang Zhao[1], Liang Zuo[1, 6, *]

[1]*Key Laboratory for Anisotropy and Texture of Materials (Ministry of Education), Northeastern University, Shenyang 110819, China.*

[2]*Laboratoire d'Étude des Microstructures et de Mécanique des Matériaux (LEM3), CNRS UMR 7239, Université de Lorraine, 57045 Metz, France.*

[3]*Laboratory of Excellence on Design of Alloy Metals for low-mAss Structures (DAMAS), Université de Lorraine, 57045 Metz, France.*

[4]*División Multidisciplinaria, Ciudad Universitaria, Universidad Autónoma de Ciudad Juárez (UACJ), calle José de Jesús Macías Delgado # 18100, Ciudad Juárez 32579, Chihuahua, México.*

[5]*Instituto Potosino de Investigación Científica y Tecnológica, Camino a la Presa San José 2055, Col. Lomas 4ª, San Luis Potosí, S.L.P. 78216, Mexico.*

[6]*Taiyuan University of Science and Technology, Taiyuan 030024, China.*

\* Corresponding Author:

Liang Zuo, Email: **lzuo@mail.neu.edu.cn** ;

J.L. Sánchez Llamazares, Email: **jose.sanchez@ipicyt.edu.mx**

## ASTRACT

The properties related to magnetocaloric effect (MCE) of annealed Ni$_{50}$Mn$_{18}$Cu$_7$Ga$_{25}$ ribbons were studied in connection with their microstructural features and magnetostructural transformations. The differences in magnetic entropy change between the reverse and direct austenite-to-martensite transformation processes lie in the availability of magnetic field induced martensitic transformation. This transformation is temperature and magnetic field dependent, *i.e.* it is attainable during the direct transformation but not reciprocal in the reverse transformation, and it occurs during the field-up process but is not reversible during the field-down process. These transformation singularities have a deep connection with the microstructural configurations of the parent and product phases. The present study provides fundamental information necessary to understand the transformation dependent MCE of ferromagnetic functional alloys.

**Keywords:** Ni–Mn–Ga; Ribbons; Magnetocaloric effect; Martensitic transformation

# 1 Introduction

The magnetocaloric effect (MCE) is characterized by the isothermal magnetic entropy change or the adiabatic temperature variation induced by the application (or removal) of an external magnetic field across a first- or second-order transition [1]. Based on this phenomenon, a new type of refrigeration technology is being developed which is more energy-efficient and environment-friendly if compared with the conventional ones based on gas compression/expansion [1,2]. Recently, Ni–Mn–X based Heusler-type ferromagnetic alloys (with X = Ga, In, and Sn) those undergo martensitic transformation (MT) and magnetic transition [3-6] are found to exhibit significant magnetocaloric (MC) properties [4,7,8]. As these alloys are less expensive than those based on rare earth elements and some of them possess a giant tunable MCE around or above room temperature, they have been considered as potential magnetic refrigerants [9-11]. Among the Ni–Mn–X families, Ni–Mn–Ga alloys have been intensively studied in view of their relatively low field-induced magnetic hysteresis losses [12,13].

For Ni–Mn–Ga based alloys, the reverse structural transformation from martensite (MST) to austenite (AST) occurs upon heating. As the martensitic and magnetic transition temperatures of these materials are sensitive to chemical composition [14,15], it is possible to adjust the composition to allow the co-occurrence of the structural and magnetic transformations (*i.e.*, the accomplishment of a magneto-structural transformation) [16], thus giving rise to an abrupt magnetization change $\Delta M$ with the consequent maximization of the MCE [7]. That is the case of stoichiometric $Ni_2MnGa$ polycrystalline alloys when Cu replaces a proper amount of Mn. A large magnetic entropy change ($\Delta S_M$) value of $-64$ Jkg$^{-1}$K$^{-1}$ under the magnetic field change $\mu_o\Delta H$ of 5 T has been achieved [17], which is not far from the highest $\Delta S_M = -86$ Jkg$^{-1}$K$^{-1}$ obtained in a $Ni_{55}Mn_{20}Ga_{25}$ single crystal [7]. Other than composition adjustment to achieve large MCE in Ni–Mn–Ga based alloys, efforts have also been made on activating additional structural transformation alongside the magnetostructural transformation [18], to further enhance the maximum magnetic entropy change $|\Delta S_M^{max}|$.

Despite the efforts in achieving high $|\Delta S_M^{max}|$, the transformation processes on both heating and cooling have not yet been explored in connection with the obtained $\Delta S_M(T)$ curves. Although the magnetostructural transformation is reversible, the direct martensitic transformation upon cooling and the reverse martensitic transformation upon heating are not exactly reciprocal [19] in terms of microstructural evolutions and the effect of the magnetic field. Thus, the MCE associated properties,

such as the temperature dependence of the magnetic entropy change and hysteresis loss, should be different. The interrelationship between them is useful for a better understanding of the effect of processing parameters on the resulting MCE behaviors.

Recently, we have studied the influence of Cu addition on the martenstic and magnetic transitions in $Ni_{50}Mn_{25-x}Cu_xGa_{25}$ (x = 0-7) melt-spun ribbons [20]. It is found that the martensitic transformation and the magnetic transition are coupled when the Cu content is up to x = 7. The field-induced martensitic transformation from a paramagnetic austenite to a ferromagnetic martensite has been realized. In this work, we focus on the transformation process dependent MCE properties in Cu-doped Ni–Mn–Ga ribbons with coupled magnetic and structural transformations. The emphasis is not to achieve the largest possible magnetic entropy change of the studied alloy, but to establish relations between the MCE associated properties with the transformation process and offer fundamental information on MCE of these ferromagnetic Ni–Mn based alloys.

## 2 Experiments

Bulk arc-melted polycrystalline alloys with nominal composition of $Ni_{50}Mn_{25-x}Cu_xGa_{25}$ (x = 0-7) were prepared using high purity raw materials in Ar atmosphere. The as-cast ingots were remelted four times to obtain good starting composition homogeneity. With a single-roller melt-spinning system, the melt-spun ribbons were fabricated at a wheel speed of 20 ms$^{-1}$. To reduce crystal defects and increase atomic ordering, they were annealed under vacuum at 1173 K for 24 hr and air-cooled to the room temperature. The starting and finishing martensitic transformation (direct and reverse) temperatures (hereafter referred as $M_s$, $M_f$, $A_s$, $A_f$) were measured by differential scanning calorimetry (DSC, TA-Q100) in the temperature range between 183 K and 473 K under a cooling and heating sweep rate of 10 Kmin$^{-1}$. The phase identification was performed at room temperature by X-ray diffraction (XRD) with Cu-$K_\alpha$ radiation. The microstructural characterizations were conducted in a field-emission-gun scanning electron microscope (SEM, Jeol JMF6500-F) with an electron backscatter diffraction (EBSD) system. The magnetic properties were measured with a physical property measurement system (Quantum Design, PPMS® EverCool®-9T). The magnetic field was applied along the longitudinal direction of the ribbons (*i.e.* the rolling direction) to minimize the internal demagnetizing field. The low-field (5 mT) magnetization was measured as a function of temperature *M* (*T*) curve between 200 K and 400 K. This was done by first cooling one sample from

room temperature to 200 K under a zero applied magnetic field; then, the magnetic field was set and the magnetization was measured at a temperature sweep rate of 1 Kmin$^{-1}$ from 200 K to 400 K (ZFC process), and *vice versa* (FC process). "Considering that the shape of the isothermal magnetization $M(\mu_o H)$ curves may strongly depends on the thermal history in the temperature range where structural phase transformation occurs thus affecting the shape of the $\Delta S_M(T)$ curves, we have followed a fixed thermal protocol to reach each measuring temperature $T_{meas}$ throughout MST → AST (AST → MST) transition [REFERENCE: A. Quintana-Nedelcos, J.L. Sánchez Llamazares, C.F. Sánchez-Valdés, P. Álvarez-Alonso, P. Gorria, P. Shamba, N.A. Morley, J. Alloys Compd. Vol. 694 (2017) 1189]: at zero magnetic field the sample is heated (cooled) to 400 K (200 K) to stabilize austenite (martensite), cooled (heated) to 200 K (400 K) to completely form martensite (austenite), and then heated (cooled) again in no-overshot mode to the selected measuring temperature $T_{meas}$. This procedure is repeated for each $T_{meas}$ because ensures that prior to apply the magnetic field the sample shows the phase constitution that correspond to the thermally induced structural transition."

## 3. Results

Among all the fabricated ribbons, the structural and magnetic transition temperatures of the annealed $Ni_{50}Mn_{18}Cu_7Ga_{25}$ ribbon were detected to be the closest [20]. Therefore, the annealed $Ni_{50}Mn_{18}Cu_7Ga_{25}$ ribbon was selected to be the focus of the present study. Fig. 1 shows the heating and cooling DSC scans and $M(T)$ curves of the ribbon under a weak magnetic field of 5 mT. The magnetic transition temperatures on heating ($T_C^{heating}$) and cooling ($T_C^{cooling}$) processes were determined from the minimum of the corresponding $dM/dT$ versus $T$ curve, as shown at the inset of Fig. 1(b). Table I lists the structural and magnetic transition temperatures of the studied $Ni_{50}Mn_{18}Cu_7Ga_{25}$ ribbon. It can be seen that $T_C^{heating}$ is between $A_s$ and $A_f$ and $T_C^{cooling}$ is between $M_s$ and $M_f$, indicating the co-occurrence of structural transformation and magnetic transition *(i.e.* a magnetostructural transformation). Moreover, it should be noticed that the temperature interval of the direct transformation (10 K) is wider than that of the reverse transformation (8 K), suggesting that the speed of the reverse transformation is higher than that of the direct transformation.

Fig. 2(a) displays a typical backscattered electron (BSE) image taken from the annealed ribbon plane, while the inset shows a magnified microstructure of the selected region marked with the red square. It is seen that the martensite is in plate shape and organized in colonies or groups within one original austenite grain. The plates within each colony stretch approximately in the same direction. It

should be noted that the thickness of the martensite plates is not uniform and some plates are much thicker than the others in some initial austenite grains. To identify the phase constitution of the annealed ribbon, EBSD measurements were performed in two selected areas (region 1 and 2), as shown in Fig. 2(b1) and Fig. 2(b2). It is observed that the thicker plates are of non-modulated (NM) martensite and the thin plates are of 7M modulated martensite. Further observations confirm that one NM plate contains two orientation variants that are twin related, as shown in the inset of Fig. 2(a), whereas one 7M plate contains only one orientation variant, which is in coincidence with what observed in bulk Ni–Mn–Ga alloys [21]. Such a microstructural configuration with co-existing 7M and NM martensites indicates that the ribbon involves two structural transformations, *i.e.* the martensitic transformation from austenite to 7M martensite and the intermartensitic transformation from 7M martensite to NM martensite, as found in a bulk $Ni_{53}Mn_{22}Ga_{25}$ alloy [22]. Together with the thermo-magnetic measurements, it can be inferred that the magnetic transition is coupled with a two-step structural transformation (austenite – 7M – NM). Moreover, the simultaneous two-step structural transformation gives rise to a large amount of inter-plate and intra-plate interfaces. Such factors surely exert considerable influence on the transformation related magnetic properties of this alloy. As the microstructural evolution in the direct transformation is not completely the reciprocal process of that in the reverse transformation, a different magnetocaloric behavior could be expected.

Figs. 3(a) and (b) show the isothermal magnetization curves $M$ ($\mu_o H$) of the $Ni_{50}Mn_{18}Cu_7Ga_{25}$ ribbon measured over the heating and cooling processes up to 5 T, where the measuring temperatures are indicated. It is considered that in the temperature range across phase transformation, the shape of the $M$ ($\mu_o H$) curves may strongly depend on the thermal history followed to reach the measuring temperature $T_{meas}$. Here, the following thermal loop was set at zero field, throughout the direct (reverse) martensitic transformation: (1) cooling (heating) to 250 K (370 K) to stabilize martensite (austenite), (2) heating (cooling) to 370 K (250 K) to completely form austenite (martensite), and (3) cooling (heating) to the selected $T_{meas}$. This procedure was repeated for each $T_{meas}$ since it ensured that, prior to applying the magnetic field at a given $T_{meas}$, the sample had consistently the phase constitution corresponding to the thermally induced structural transition. For the heating process (Fig. 3(a)), the shapes of the curves change from that of typical ferromagnetism (below 315 K) to that of paramagnetism (above 325 K), and in between the isotherms exhibit a nearly linear dependence without saturation. However, for the cooling process (Fig. 3 (b)), the curves are quite different in shape. As shown in the figure, the signature of a field-induced meta-magnetic behavior is clearly identified in the temperature range from 315 K to 324 K, *i.e.* a sudden change in the slope at a given critical magnetic field $\mu_o H_{cr}$ with the consequent fast and progressive increase in magnetization. This indicates the occurrence of a field-induced martensitic transformation from a paramagnetic austenite to a ferromagnetic martensite. With the decrease of the temperature, the critical magnetic field

decreases.

From the isothermal magnetization curves, we calculated the thermal dependence of the magnetic entropy change through numerical integration of the Maxwell relation [23]. The $\Delta S_M(T)$ curves for the heating and cooling processes under a magnetic field of 2 T and 5 T are shown in Fig. 3 (c) and (d), respectively. For $\mu_o\Delta H= 5$ T, $\Delta S_M^{max}$ reaches values of –32.1 Jkg$^{-1}$K$^{-1}$ and 17.8 Jkg$^{-1}$K$^{-1}$ for the reverse and direct transformations, respectively. Note that the $|\Delta S_M^{max}|$ through the reverse transformation is higher than that of the annealed Ni$_{52}$Mn$_{26}$Ga$_{22}$ ribbons (30.0 Jkg$^{-1}$K$^{-1}$) reported in Ref. [13]. From the $\Delta S_M(T)$ curves, it is seen that the peaks appear at the vicinity of 323 K and 318 K for the reverse and direct transformations, respectively. These temperatures are close to the magnetostructural transformation temperature, indicating that the $|\Delta S_M^{max}|$ results from the coupled magnetic and structural transitions. However, the shapes of both $\Delta S_M(T)$ curves and the peak values reached are quite different. The peak shapes for the reverse transformation are similar for 2 T and 5 T and the peak positions roughly appear at the same temperature, whereas the peak shape of the direct transformation under 5 T is wider than that under 2 T and the peak position appears at higher temperature.

Table II lists the $|\Delta S_M^{max}|$ values at 2 T and 5 T and the relative increase with the field change ($\left(\frac{|\Delta S_M^{max}|^{5T}}{|\Delta S_M^{max}|^{2T}}-1\right)\times100\%$) for the direct and reverse transformations. It is seen that $|\Delta S_M^{max}|$ increases with the increase of the applied magnetic field change for both direct and reverse transformation, but the absolute values reached are quite different. $|\Delta S_M^{max}|$ for the reverse transformation under 2 T is 11.9% lower than that of the direct transformation, whereas the value from the reverse transformation under 5 T is 80.3% higher than that of the direct transformation. Moreover, the increases in $|\Delta S_M^{max}|$ induced by the increased field for the two directional transformations are also very different. For the direct transformation, $|\Delta S_M^{max}|$ is only increased by 24.5% from 2 T to 5 T, whereas for the reverse transformation, it is increased by 154.7%. With the increase of $\mu_o\Delta H$, the $|\Delta S_M^{max}|$ undergoes a drastic increase for the reverse transformation. The $|\Delta S_M^{max}|$ versus $\mu_o\Delta H$ plots are shown at the insets of Figs. 3 (c) and (d) to highlight the almost linear and parabolic dependence for the reverse and the direct transformations.

Considering that the hysteresis losses diminish the useful entropy that can be used for cooling purpose in the temperature range determined by the full-width at half maximum of the $\Delta S_M(T)$ curve $\delta T_{FWHM}= T_{hot} - T_{cold}$, we made corresponding measurements across the reverse and direct transitions at 2 T and 5 T. The hysteresis loss at a given temperature has been estimated from the area enclosed between the magnetization isotherms measured by applying and removing a magnetic field. Fig. 4 (a) to (d) present the set of isothermal magnetization curves $M(\mu_oH)$ measured with such a purpose for

the reverse and direct transformations. It should be noted that the shapes of the field-up and field-down curves are quite different for both transformations, indicating a different nature of the field-induced transformation, which, in turns, leads to different magnitudes of the magnetic hysteresis. For the direct transformation the meta-magnetic transition leads to large hysteresis losses because austenite is irreversibly transformed into martensite, whereas for the reverse one no critical magnetic field can be located and the transformation is gradual and smooth. The thermal dependences of the hysteresis loss across both transformations are displayed in Fig. 4 (e) and (f), respectively, where the temperature ranges corresponding to the $\delta T_{FWHM}$ of the $\Delta S_M$ at 2 T and 5 T are indicated. For the reverse (direct) transformation, the maximum values of the hysteresis loss under 2 T and 5 T are 2.2 (19.0) Jkg$^{-1}$ and 11.2 (43.0) Jkg$^{-1}$. Clearly, the direct transformation generates much higher hysteresis loss. Moreover, the temperature ranges $\delta T_{FWHM}$ for the reverse transformation at respectively 2 T and 5 T are located at the beginning of the ramparts of the hysteresis loss curves and the peak values of the hysteresis loss curves are out of the $\delta T_{FWHM}$ ranges. This suggests that the adversary contribution of the hysteresis loss to the MCE effect is small for the reverse transformation. However, the situation for the direct transformation is quite different. The peak values of the hysteresis loss curves are within the $\delta T_{FWHM}$ temperature ranges of the $\Delta S_M$ ($T$) curves. Therefore, the MCE effect is affected to a large extent by the hysteresis loss.

# 4 Discussion

The above results have demonstrated that the MCE of the presently studied ribbon, which is maximized owing to the concomitant structural transformation and magnetic transition, shows significant differences over both direct and reverse transitions. These differences are strongly related to the magnetic nature of the product phase of the transformation, namely a ferromagnetic (paramagnetic) martensite (austenite) for the direct (reverse) transformation. With an external magnetic field, the change of the magnetization of martensite is not linear. The magneitzation increases quickly at low field and reaches saturation, whereas the increase of the magnetization of austenite is linear but there is no saturation. As the martensite and austenite phases are respectively strongly and weakly magnetic, the direct transformation that happens below $M_s$, will be promoted to a temperature higher than $M_s$ by the so-called magnetic field-induced transformation, as evidenced by the isothermal magnetization curves in Fig. 4(b). However, for the reverse transformation that

happens above $A_s$ (higher than $M_s$), the magnetic field does not show any effect.

Considering that the maximum entropy change curve depends largely on $(\partial M/\partial T)|_{\mu_o H}$, we plot the $(\partial M/\partial T)|_{\mu_o H}$ curves for both direct and reverse transformations, as shown in Fig. 5. In the present case, $(\partial M/\partial T)|_{\mu_o H}$ at a given temperature represents the magnetization gradient within the corresponding temperature interval $\Delta T$ (defined by a higher and a lower temperature limit). This magnetization gradient results from the different volume fractions of martensite (Mar%) and austenite (Aus%) between two temperature limits, as well as the different magnetization behaviors of the ferromagnetic martensite and the paramagnetic austenite under an applied magnetic field. During the reverse transformation, Mar% decreases and Aus% increases with the increasing temperature. The decrement of Mar% and the increment of Aus% between every pair of higher and lower temperature limits (with equal temperature interval) firstly enhance and then reduce with the progress of the transformation from low temperature to high temperature, according to the kinetic characters of martensitic transformation [19]. As a result, the magnitude of $(\partial M/\partial T)|_{\mu_o H}$ increases when the transformation temperature is low where the volume variation of martensite is dominant and decreases when the transformation temperature is high where the volume variation of martensite is reduced and the amount of austenite becomes dominant. At a given temperature, the behavior of $(\partial M/\partial T)|_{\mu_o H}$ at low magnetic field is dominated by ferromagnetism (non linear variation) where the magnetization variation from paramagnetic austenite is nearly negligible, whereas at high magnetic field the behavior of $(\partial M/\partial T)|_{\mu_o H}$ is dominated by paramagnetic behavior (linear variation) where the magnetization from ferromagnetic martensite is constant due to magnetization saturation. Hence, the $(\partial M/\partial T)|_{\mu_o H}$ versus $\mu_o H$ curves do not show any saturation for the whole field span, as shown in Fig. 5 (a). However, for the direct transformation, the shape and the maximum value of the $(\partial M/\partial T)|_{\mu_o H}$ curve (Fig. 5 (b)) is quite different from those of the reverse transformation (Fig. 5 (a)). The curves exhibit a typical Gaussian shape with a well-defined peak value on the field intensity scale due to the occurrence of the temperature dependent field-induced martensitic transformation. One can think that at the lower limit of a certain temperature interval, when the magnetic field value is over the critical field value, austenite starts to transform to martensite, but at the higher temperature limit the transformation does not proceed under the same magnetic field. In this way, the $(\partial M/\partial T)|_{\mu_o H}$ corresponding to this temperature interval increases drastically due to the increase of Mar% at the lower temperature limit. However, with the continuous increase of the magnetic field, the field-induced transformation moves to higher temperature and the field-induced transformation starts at

higher temperature limit when the field is sufficient. As a result, the Mar% of the two temperature limits quickly approaches to the same amount, and the $(\partial M/\partial T)\vert_{\mu_o H}$ at this temperature interval quickly decreases, resulting in a Gaussian shaped curve. As the field-induced transformation is temperature dependent, the peak of $(\partial M/\partial T)\vert_{\mu_o H}$ shifts from the high-field region to a lower field region when the temperature decreases. Due to the fact that the field-induced transformation happens only during the direct transformation, the reverse and the direct transformations are not reciprocal with respect to either the temperature or the magnetic field. During the reverse and the direct transformations, $(\partial M/\partial T)\vert_{\mu_o H}$ behaves very differently with the magnetic field, thus resulting in non symmetrical temperature resolved $\Delta S_M$ of the two directional transformations in terms of the peak shape, peak value and peak position. In terms of $\vert \Delta S_M^{max}\vert$, the reverse transformation provides a higher value, because $(\partial M/\partial T)\vert_{\mu_o H}$ has a slow variation with the magnetic field and thus large effective integration range.

The $\delta T_{FWHM}$ of the $\Delta S_M (T)$ curve represents the working temperature range. This width is clearly related to the field-induced martensitic transformation that occurs during the direct transformation, since the width broadening with the increase of magnetic field happens exclusively in the process of direct transformation. This can be explained by the fact that the temperature dependent field-induced transformation makes the $(\partial M/\partial T)\vert_{\mu_o H}$ peak shift toward low field region when temperature drops within the temperature interval where the direct transformation could be induced (Fig. 5 (b)). As a result, the $\Delta S_M$ peak that is the integration of $(\partial M/\partial T)\vert_{\mu_o H}$ against magnetic field is broadened with magnetic field, and so does the $\delta T_{FWHM}$, as shown in Fig. 4 (d). Thus, any treatments that broaden the $\Delta S_M$ peak (large $\delta T_{FWHM}$) of the magnetic refrigeration materials should be effective approaches not only to optimize their useful cooling entropy but also to obtain a wide working temperature range.

As average hysteresis loss within the $\delta T_{FWHM}$ of the $\Delta S_M (T)$ curve diminishes the useful entropy that can be used for cooling purposes, we list the maximum loss and the average loss within this temperature interval of the $\delta T_{FWHM}$ in Table II. The average hysteresis losses in the reverse transformation are much smaller than those in the direct transformation due to the different possibilities of the field-induced martensitic transformation for the two directional transformations and the different microstructural factors created during the two processes. As evidenced by microstructural observations, the austenite is in equiaxed shape, as schematically represented in Fig. 6. When it transforms into martensite, the transformation involves not only the change of crystal structure but also the formation of large amount of interfaces (martensite plate interfaces and colonies

interfaces). Moreover, a volume fraction of the 7M martensite continues to transform into NM martensite, forming lamellar interfaces within each NM plate, as represented in Fig. 6. Such microstructural configurations impose difficulty for a reverse transformation to the initial austenite state when the magnetic field is removed. Large magnetization difference is created between the magnetization and demagnetization process, thus resulting in large hysteresis. Additionally, the non-coincidence of the hysteresis loss peak with the $\delta T_{FWHM}$ of the $\Delta S_M$ peak in the temperature scale for the reverse transformation eliminates the adverse contribution of the hysteresis loss to the MCE effect.

# 5 Summary

In the present work, simultaneous magnetic transition and structural transformation, *i.e.* the magnetostructural transformation, was achieved for Ni–Mn–Ga ribbons by Cu doping with a nominal composition of $Ni_{50}Mn_{18}Cu_7Ga_{25}$. The magnetocaloric properties in terms of $\Delta S_M$ and hysteresis loss of the annealed ribbon were studied in connection with microstructural characterizations and transformation process analyses. There are clear differences between the reverse transformation (martensite to austenite in heating process) and the direct transformation (austenite to martensite in cooling process). The discrepancy is deeply related to the martensitic transformation induced by magnetic field that has two specific features. The first is that it occurs uniquely during the direct transformation and is temperature dependent. The second is that it is not reversible when the field is removed. As a result, the maximum $\Delta S_M$ value is higher (–32.1 $Jkg^{-1}K^{-1}$ versus –17.8 $Jkg^{-1}K^{-1}$ under 5 T) but the $\delta T_{FWHM}$ of the $\Delta S_M$ peak is smaller (3 K versus 6 K under 5 T) for the reverse transformation with respect to those of the direct transformation. Due to the non reciprocal microstructural evolution during cooling and heating process between austenite (in equiaxed grains) and martensite (in plate and lamellar shapes), the field induced martensitic transformation is not reversible when the field is removed during the direct transformation, resulting in much larger magnetic hysteresis. This study provides fundamental information on transformation process dependent MCE of Ni–Mn–Cu–Ga alloys in relation with microstructural features. The results obtained by this work could be useful to understand the MCE behaviors of ferromagnetic functional alloys.

# Acknowledgements

# References

[1] Vitalij K. Pecharsky, and Karl A. Gschneidner Jr, Magnetocaloric effect and magnetic refrigeration, J. Magn. Magn. Mater. 200 (1999) 44-56.

[2] J. Glanz, Making a bigger chill with magnets, Science 279 (1998) 2045.

[3] L. Pareti, M. Solzi, F. Albertini, and A. Paoluzi, Giant entropy change at the co-occurrence of structural and magnetic transitions in the Ni Mn Ga Heusler alloy, Eur. Phys. J. B 32 (2003) 303.

[4] T. Krenke, E. Duman, M. Acet, E.F. Wassermann, X. Moya, L. Mañosa, and A. Planes, Inverse magnetocaloric effect in ferromagnetic Ni–Mn–Sn alloys, Nature Mater. 4 (2005) 450.

[5] T. Krenke, X. Moya, S. Askoy, M. Acet, P. Entel, Ll. Mañosa, A. Planes, Y. Elerman, A Yücel, and E.F. Wassermann, Electronic aspects of the martensitic transition in Ni–Mn based Heusler alloys, J. Magn. Magn. Mater. 310 (2007) 2788.

[6] I. Dubenko, M. Khan, A.K. Pathak, B.R. Gautam, S. Stadler, and N. Ali, Magnetocaloric effects in Ni–Mn–X based Heusler alloys with X= Ga, Sb, In, J. Magn. Magn. Mater. 321 (2009) 754.

[7] M. Pasquale, C.P. Sasso, L.H. Lewis, L. Giudici, T. Lograsso, and D. Schlagel, Magnetostructural transition and magnetocaloric effect in Ni 55 Mn 20 Ga 25 single crystals, Phys. Rev. B 72 (2005) 094435.

[8] X.X. Zhang, M.F. Qian, R.Z. Su, and L. Geng, Giant room-temperature inverse and conventional magnetocaloric effects in Ni–Mn–In alloys, Mater. Lett. 163 (2016) 274-276.

[9] Z.D. Han, D.H. Wang, C.L. Zhang, H.C. Xuan, B.X. Gu, and Y.W. Du, Low-field inverse magnetocaloric effect in $Ni_{50-x}Mn_{39+x}Sn_{11}$ Heusler alloys, Appl. Phys. Lett. 90 (2007) 042507.

[10] Z.D. Han, D.H. Wang, C.L. Zhang, S.L. Tang, B.X. Gu, and Y.W. Du, Large magnetic entropy changes in the $Ni_{45.4}Mn_{41.5}In_{13.1}$ ferromagnetic shape memory alloy, Appl. Phys. Lett. 89 (2006) 182507.

[11] J. Liu, T. Gottschall, K.P. Skokov, J.D. Moore, and O. Gutfleisch, Giant magnetocaloric effect driven by structural transitions, Nature Mater. 11 (2012) 620-626.

[12] Z.B. Li, J.L. Sánchez Llamazares, C.F. Sánchez-Valdés, Y.D. Zhang, C. Esling, X. Zhao, and L. Zuo, Microstructure and magnetocaloric effect of melt-spun $Ni_{52}Mn_{26}Ga_{22}$ ribbon, Appl. Phys. Lett. 100 (2012) 174102.

[13] Z.B. Li, Y.D. Zhang, C.F. Sánchez-Valdés, J.L. Sánchez Llamazares, C. Esling, X. Zhao, and L. Zuo, Giant magnetocaloric effect in melt-spun Ni-Mn-Ga ribbons with magneto-multistructural transformation, Appl. Phys. Lett. 104 (2014) 044101.

[14] V.A. Chernenko, Compositional instability of β-phase in Ni-Mn-Ga alloys, Scr. Mater. 40 (1999) 523.

[15] X. Moya, L. Mañosa, A. Planes, T. Krenke, M. Acet, and E.F. Wassermann, Martensitic transition and magnetic properties in Ni–Mn–X alloys, Mater. Sci. Eng. A 438-440 (2006) 911-915.

[16] N.V. Rama Rao, R. Gopalan, M. Manivel Raja, J. Arout Chelvane, B. Majumdar, and V. Chandrasekaran, Magneto-structural transformation studies in melt-spun Ni–Mn–Ga ribbons, Scr. Mater. 56 (2007) 405-408.

[17] S. Stadler, M. Khan, J. Mitchell, N. Ali, A.M. Gomes, I. Dubenko, A.Y. Takeuchi, and A.P.

Guimarães, Magnetocaloric properties of $Ni_2Mn_{1-x}Cu_xGa$, Appl. Phys. Lett. 88 (2006) 192511.

[18] Z. Li, K. Xu, Y.L. Zhang, C. Tao, D. Zheng, and C. Jing, Two successive magneto-structural transformations and their relation to enhanced magnetocaloric effect for $Ni_{55.8}Mn_{18.1}Ga_{26.1}$ Heusler alloy, Sci. Rep. 5 (2015) 15143.

[19] E. Patoor, D.C. Lagoudas, P.B. Entchev, L.C. Brinson, and X. Gao, Shape memory alloys, Part I: General properties and modeling of single crystals, Mechanics of Materials 38 (2006) 391-429.

[20] Z.B. Li, N.F. Zou, C.F. Sánchez-Valdés, J.L. Sánchez Llamazares, B. Yang, Y. Hu, Y.D. Zhang, C. Esling, X. Zhao, and L. Zuo, Thermal and magnetic field-induced martensitic transformation in $Ni_{50}Mn_{25-x}Ga_{25}Cu_x$ ($0 \leqslant x \leqslant 7$) melt-spun ribbons, J. Phys. D: Appl. Phys. 49 (2016) 25002-25007.

[21] D.Y. Cong, Y.D. Zhang, Y.D. Wang, C. Esling, X. Zhao, and L. Zuo, Determination of microstructure and twinning relationship between martensitic variants in 53 at.% Ni–25 at.% Mn–22 at.% Ga ferromagnetic shape memory alloy, J. Appl. Cryst. 39 (2006) 723-727.

[22] Z.B. Li, B. Yang, Y.D. Zhang, C. Esling, N.F. Zou, X. Zhao, and L. Zuo, Crystallographic insights into the intermartensitic transformation in Ni–Mn–Ga alloys, Acta Mater. 74 (2014) 9-17.

[23] A.M. Tishin and Y.I. Spichkin, The Magnetocaloric Effect and Its Applications IOP, New York (2003).

Captions of table and figure:

Table 1    Starting and finishing temperatures of reverse ($A_s$, $A_f$) and direct ($M_s$, $M_f$) martensitic transformation and temperatures of magnetic transition ($T_C$) on cooling and heating for $Ni_{50}Mn_{18}Cu_7Ga_{25}$ ribbon, determined respectively from DSC and low-field $M$ ($T$) curves.

Table 2    $|\Delta S_M^{max}|$, $\delta T_{FWHM}$, maximum ($HL^{max}$) and average ($<HL>$) hysteresis losses through the reverse and direct martensitic transformation under magnetic field changes of 2 T and 5 T for $Ni_{50}Mn_{18}Cu_7Ga_{25}$ ribbon.

Fig. 1    DSC curves (a) and $M$ ($T$) curves (b) of the annealed $Ni_{50}Mn_{18}Cu_7Ga_{25}$ ribbon, measured under a magnetic field of 5 mT. The inset shows the $dM/dT$ as a function of temperature ($T$).

Fig. 2    (a) BSE image of the annealed $Ni_{50}Mn_{18}Cu_7Ga_{25}$ ribbon. The inset shows the magnified image of the region marked in red square. (b) EBSD phase-indexed images of two selected regions marked in black square in (a). The phase colored in red corresponds to 7M modulated martensite and that in blue to NM martensite.

Fig. 3    (a)-(b) Isothermal magnetization curves $M(\mu_oH)$ of the annealed $Ni_{50}Mn_{18}Cu_7Ga_{25}$ ribbon during heating from 290 K to 333.5 K and during cooling from 350 K to 285 K. (c)-(d) Entropy change $\Delta S_M$ as a function of temperature during heating and cooling (Inset: peak value $\Delta S_M^{max}$ as a function of magnetic field). Temperature protocol used to measure each $M$ ($\mu_oH$) curves: heating (or cooling) to 370 K (or 250 K) and then cooling (or heating) to 250 K (or 370 K) at 0 T and then heating (or cooling) to the measurement temperature $T_{meas}$.

Fig. 4    Isothermal magnetization curves $M$ ($\mu_oH$) measured on increasing the magnetic field $\mu_oH$ up to 2 T or 5 T and on decreasing it from 2 T or 5 T for the reverse transformation (a) and (c) and the direct transformation (b) and (d), and the temperature resolved hysteresis loss for the reverse transformation (e) and the direct transformation (f) of the annealed $Ni_{50}Mn_{18}Cu_7Ga_{25}$ ribbon.

Fig. 5    Magnetic field resolved $(\partial M/\partial T)\,|_{\mu_oH}$ curves for the reverse (a) and direct (b) transformations at selected temperatures within the transformation temperature ranges.

Fig. 6    Microstructural evolution through martensitic and intermartensitic transformations: schematic representation.

Table 1 Starting and finishing temperatures of reverse ($A_S$, $A_f$) and direct ($M_S$, $M_f$) martensitic transformation and temperatures of magnetic transition ($T_C$) on cooling and heating for Ni$_{50}$Mn$_{18}$Cu$_7$Ga$_{25}$ ribbon, determined respectively from DSC and low-field $M(T)$ curves.

| $M_S$ (K) | $M_f$ (K) | $A_S$ (K) | $A_f$ (K) | $T_C$ (K) | |
|---|---|---|---|---|---|
| | | | | cooling | heating |
| 314 | 304 | 314 | 322 | 312 | 319 |

Table 2 $\Delta S_M^{max}$, $\delta T_{FWHM}$, maximum ($HL^{max}$) and average ($<HL>$) hysteresis losses through the reverse and direct martensitic transformation under magnetic field changes of 2 T and 5 T for Ni$_{50}$Mn$_{18}$Cu$_7$Ga$_{25}$ ribbon.

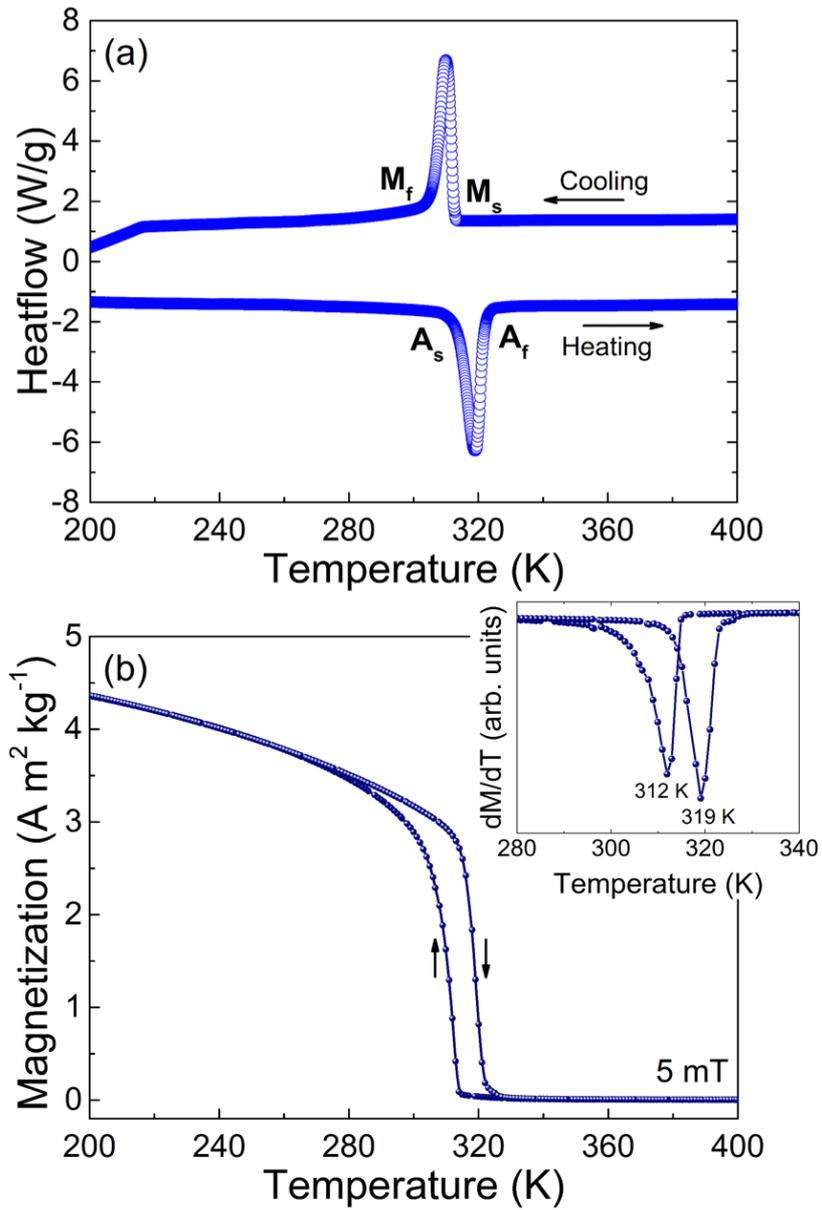| Transformation type | $\Delta S_M^{max}$ (Jkg$^{-1}$K$^{-1}$) | | $(\frac{\Delta S_M^{max 5T}}{\Delta S_M^{max 2T}} -1) \times 100$ (%) | $\delta T_{FWHM}$ (K) | | $HL^{max}$ (Jkg$^{-1}$) | | $<HL>$ (Jkg$^{-1}$) | |
|---|---|---|---|---|---|---|---|---|---|
| | 2 T | 5 T | | 2 T | 5 T | 2 T | 5 T | 2 T | 5 T |
| Reverse transformation | 12.6 | 32.1 | 155 | 3 | 3 | 2.2 | 11.2 | 0.7 | 3.3 |
| Direct transformation | -14.3 | -17.8 | 24 | 2 | 6 | 19.0 | 43.6 | 11.2 | 29.3 |

Fig. 1 DSC curves (a) and $M(T)$ curves (b) of the annealed $Ni_{50}Mn_{18}Cu_7Ga_{25}$ ribbon, measured under a magnetic field of 5 mT. The inset shows the $dM/dT$ as a function of temperature ($T$).
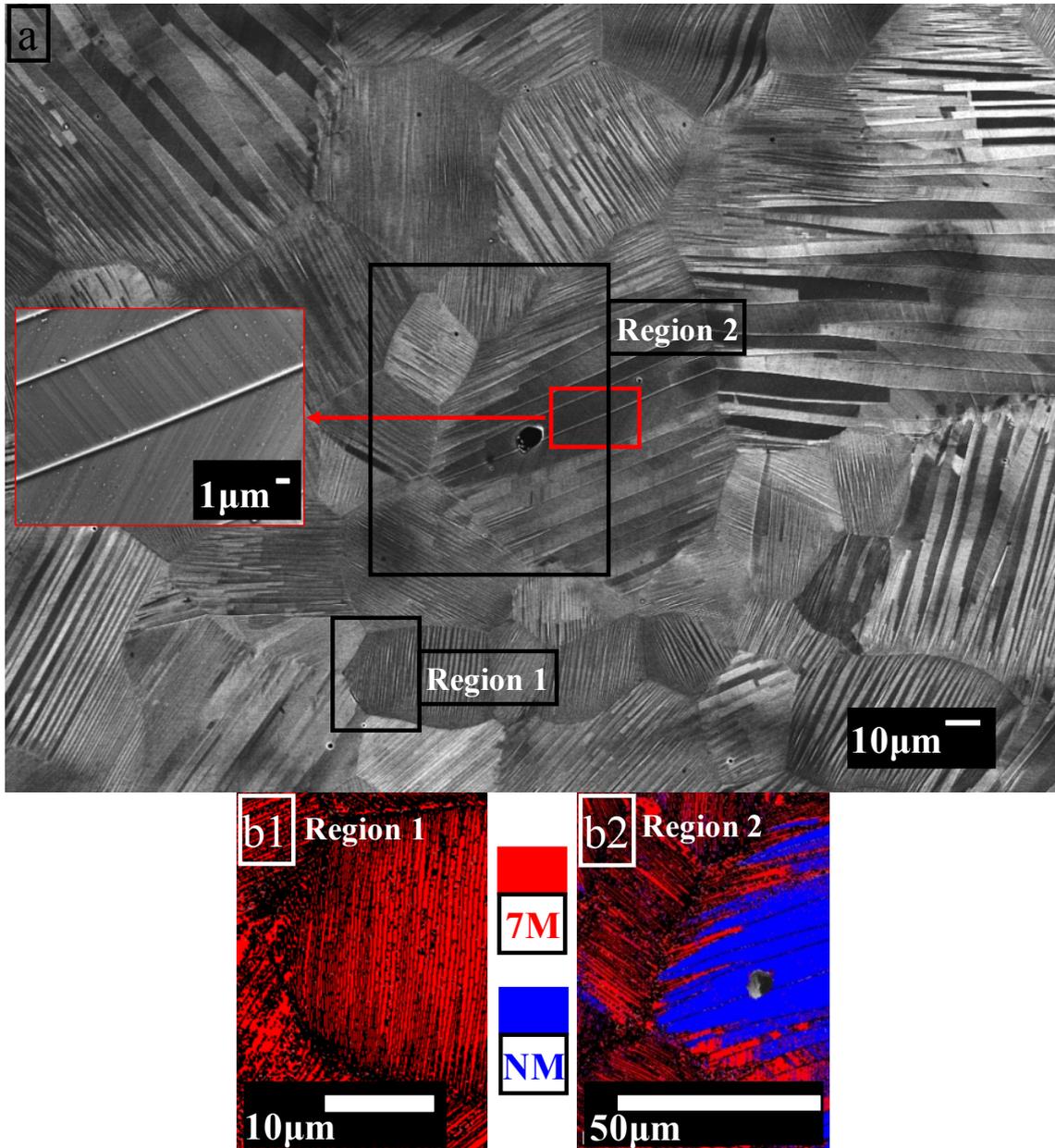
Fig. 2 (a) BSE image of the annealed $Ni_{50}Mn_{18}Cu_7Ga_{25}$ ribbon. The inset shows the magnified image of the region marked in red square. (b) EBSD phase-indexed images of two selected regions marked in black square in (a). The phase colored in red corresponds to 7M modulated martensite and that in blue to NM martensite.

Fig. 3 (a)-(b) Isothermal magnetization curves $M(\mu_o H)$ of the annealed $Ni_{50}Mn_{18}Cu_7Ga_{25}$ ribbon during heating from 290 K to 333.5 K and during cooling from 350 K to 285 K. (c)-(d) Entropy change $\Delta S_M$ as a function of temperature during heating and cooling (Inset: peak value $\Delta S_M^{max}$ as a function of magnetic field). Temperature protocol used to measure each $M(\mu_o H)$ curves: heating (or cooling) to 370 K (or 250 K) and then cooling (or heating) to 250 K (or 370 K) at 0 T and then heating (or cooling) to the measurement temperature $T_{meas}$.
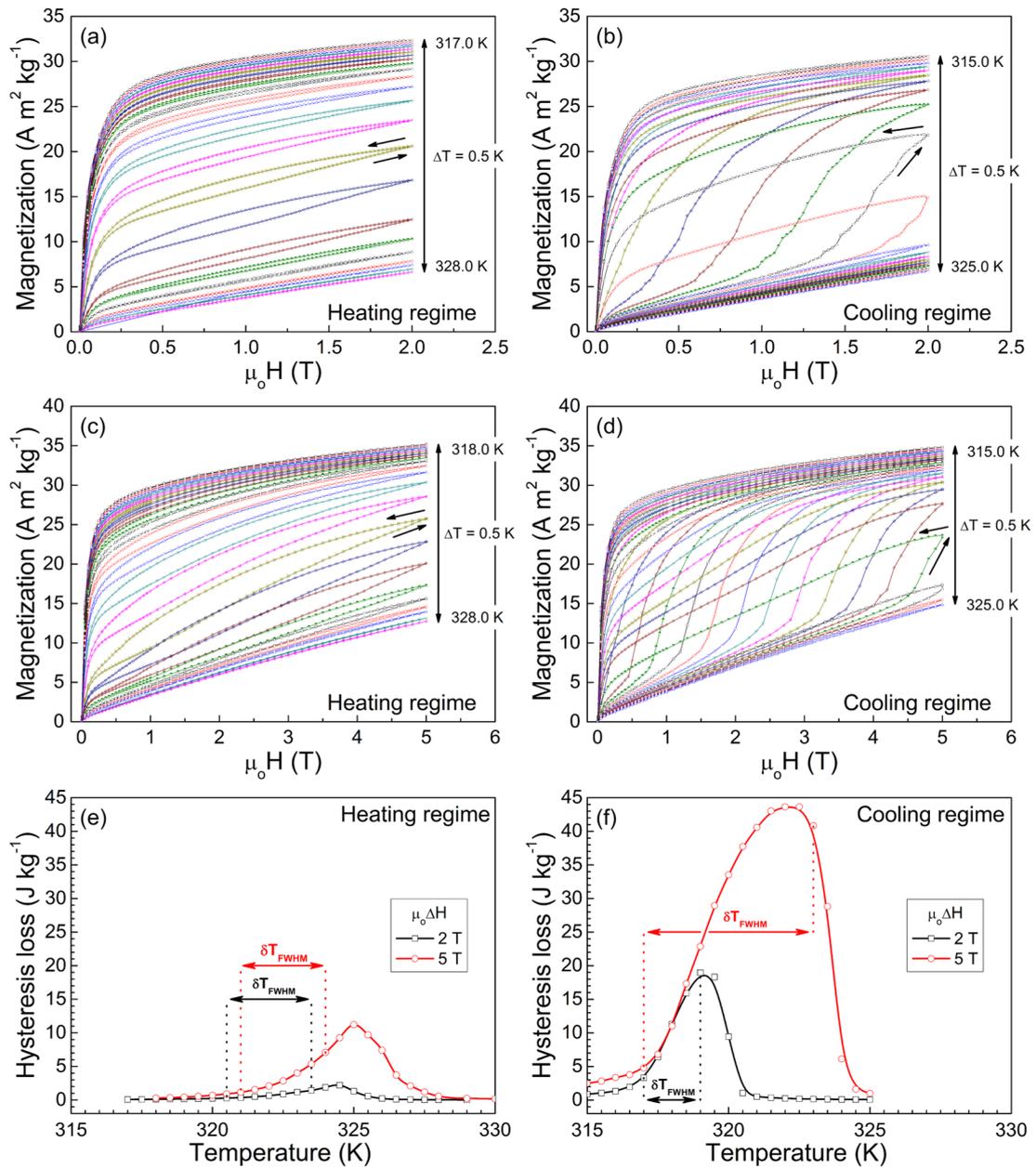
Fig. 4 Isothermal magnetization curves $M(\mu_oH)$ measured on increasing the magnetic field $\mu_oH$ up to 2 T or 5 T and on decreasing it from 2 T or 5 T for the reverse transformation (a) and (c) and the direct transformation (b) and (d), and the temperature resolved hysteresis loss for the reverse transformation (e) and the direct transformation (f) of the annealed $Ni_{50}Mn_{18}Cu_7Ga_{25}$ ribbon.
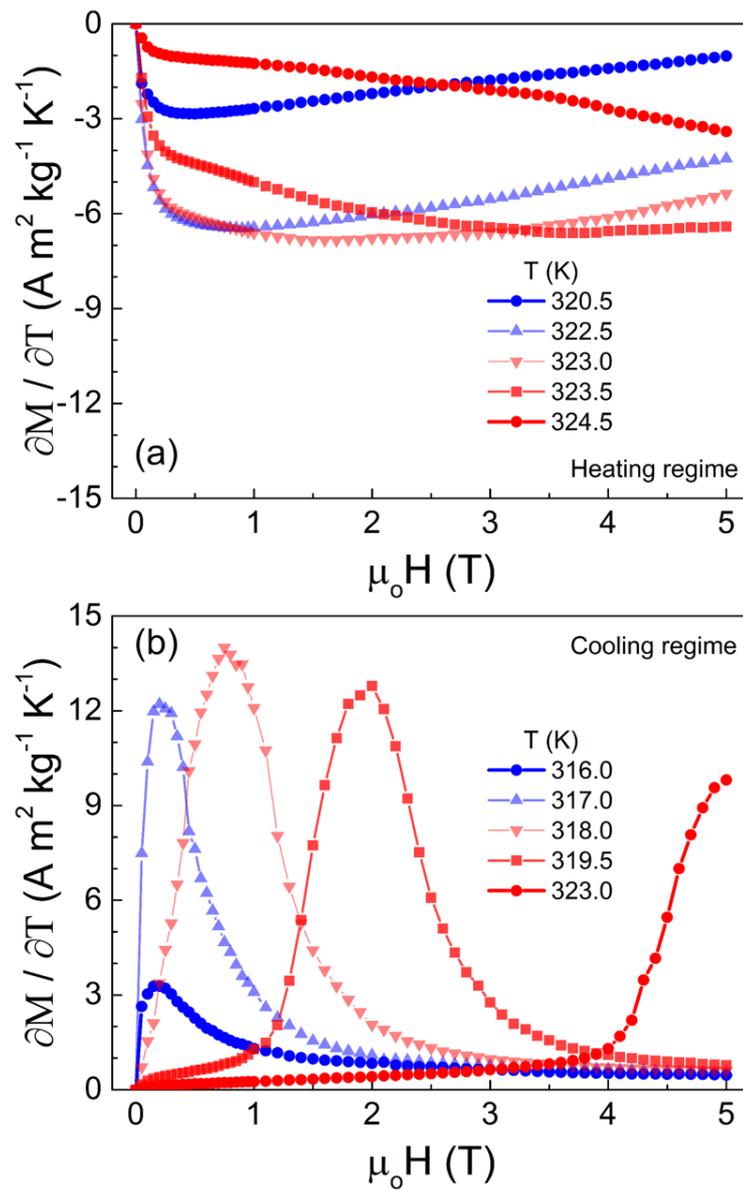
Fig. 5 Magnetic field resolved $(\partial M/\partial T)\,|_{\mu_o H}$ curves for the reverse (a) and direct (b) transformations at selected temperatures within the transformation temperature ranges.
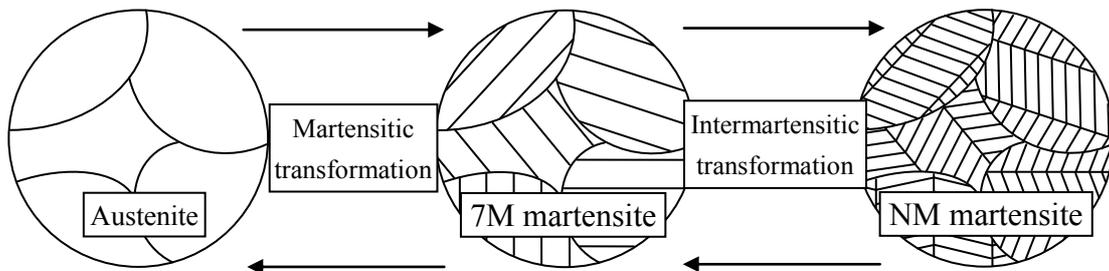


Fig. 6 Microstructural evolution through martensitic and intermartensitic transformations: schematic representation.